The International Archives of the Photogrammetry, Remote Sensing and Spatial Information Sciences, Volume L-4/W2-2026
21st International 3D GeoInfo Conference 2026, 28–29 September 2026, Sofia, Bulgaria

Bio-inspired Cutaway Visualization for Voxel-based Urban Digital Twins

Olga Shkedova[1], Udo Feuerhake[1], Stefan Fuest[1], Monika Sester[1]

[1] Institute of Cartography and Geoinformatics, Leibniz Universität Hannover, Germany - (olga.shkedova, udo.feuerhake, stefan.fuest, monika.sester)@ikg.uni-hannover.de

Keywords: Urban digital twin, Voxel representation, 3D visualization, Cutaway, Avian vision

Abstract

Ongoing urbanization has driven the development of Urban Digital Twins (UDTs) as virtual replicas of cities integrating heterogeneous data sources. While voxel-based UDTs have emerged as a promising framework for real-time applications, dense urban environments remain prone to visual clutter and occlusions, necessitating specialized visualization techniques such as cutaway approaches in order to guide the focus of the users.
Drawing inspiration from the avian visual system, this paper proposes a bio-inspired cutaway visualization for voxel-based urban environments integrating multiple visual features, including varying LOD, color contrast, transparency halo, dark tint, and magnification, to enhance focus object observation. The cutaway was evaluated through a user survey with 23 participants.
Although the bio-inspired cutaway outperformed the standard cutaway technique without additional visual variables, the average rating of 3.66 on a 5-point Likert scale (where 1 = strongly disagree, 5 = strongly agree) suggests that the approach has potential for further refinement. Future work will optimize the current visual features, explore additional visual variables, and investigate alternative interactive scenarios alongside larger-scale user studies.

1. Introduction

The rapid urbanization of the 21st century has necessitated the development of sophisticated tools for city planning, infrastructure management, and environmental monitoring. Among these tools, Urban Digital Twins (UDTs) have emerged as a significant advancement, building upon both traditional urban models, and the more recent smart-city paradigm (Ferré-Bigorra et al., 2022). Originating from product life-cycle management (Grieves and Vickers, 2017), the concept gained traction in urban contexts around 2018 to enrich semantic 3D city models with live data streams (Ruohomäki et al., 2018). Today, UDTs are defined as virtual replicas of cities that integrate heterogeneous data sources to produce comprehensive and dynamic digital representations of urban systems, and they remain fundamentally grounded in spatial data and 3D city models (Azadi et al., 2025; Schrotter and Hürzeler, 2020).

Recent advances in IoT, AI-driven data fusion, and cloud computing have increased temporal data availability for urban applications, leading to multiple UDTs for diverse use cases (Schrotter and Hürzeler, 2020; Raes et al., 2022; Lehner and Dorffner, 2020). Despite the prevalence of surface-based models like CityGML and BIM, voxel-based approaches have drawn considerable attention (Heeramaglore and Kolbe, 2022; Gorte, 2023). Voxel representations unify the urban environment within a regular 3D grid, simplifying real-time updates and simulations, while direct integration of LiDAR point clouds enables high-resolution capture of urban features such as facades, trees, fences, traffic signs, and pedestrians. Hence, a dedicated class of voxel-based UDTs has emerged for real-time applications. For instance, Mortazavi et al. (2023) proposed a voxel-based UDT for smart space management with real-time parking updates. Gorte (2023) developed a 20 cm-resolution voxel-based UDT of Hilversum using an octree-based structure to address memory limits, while Xu et al. (2026) introduced a voxel-based wildfire propagation simulator for the Wildland-Urban Interface in Newcastle, Australia.

Increasing data heterogeneity and dimensionality have raised UDT complexity, making 3D visualization essential. A core UDT feature is intuitive viewing and interaction with urban spaces (Martella et al., 2023). Despite existing visualization techniques (Cornel et al., 2019; Cárdenas-León et al., 2024; Sukma et al., 2024), dense 3D urban environments prone to visual clutter and occlusions require specialized approaches such as cutaway (Mota et al., 2026). Cutaway facilitates inspection of occluded or internal structures by selectively removing outer surfaces, enabling interactive cuts within the volumetric model to explore hidden features while preserving spatial awareness (Knödel and Guitton, 2009). Such visualization is widely demanded across UDT applications, including infrastructure monitoring, building-centric temporal analytics, and hazard simulation (Konev et al., 2018; Mota et al., 2026; Rauer-Zechmeister et al., 2024).

Visual object tracking and monitoring are essential for UDT situational awareness in traffic management, public safety, and emergency response. Despite intensive research on object detection using diverse sensor data (Vujasinović et al., 2020; Shen et al., 2025; Wang et al., 2026), interactive visualization of tracked objects in dense urban environments has received little attention. Therefore, this paper proposes a bio-inspired cutaway visualization for voxel-based urban environments that emphasizes small yet significant elements within the scene. The technique aims to track a target object and its surroundings from multiple viewpoints while preserving overall scene context. Inspired by the avian visual system, the method is designed to support focal attention through LOD representation and visual variables including transparency, color intensity, and lens magnification. The approach was applied to a static object observed from a moving viewpoint. This study represents an intermediate step toward a comprehensive real-time solution. An initial user survey evaluated the approach, identifying strengths and limitations in object recognition, tracking, and contextual awareness to guide future cutaway development for voxel-based UDTs.

2. Related work

2.1 Avian vision

The avian eye is a highly specialized sensory organ, distinguished from its mammalian counterpart by profound structural and functional adaptations that are considered to make it one of the most capable visual systems in the animal kingdom (Koncicki et al., 2025). The avian visual system comprises three distinct field components: the binocular area, which supports depth perception and prey handling through the shallow temporal fovea; the lateral area, which contains the deep central fovea, the retinal narrow high-acuity field with angular size of $\sim$1°- 2°, for detecting distant objects, while the remainder of the lateral field (peripheral vision) provides substantially lower resolution; and the blind area, which affords no visual coverage. This configuration varies across species — for instance, raptors are characterized by narrow binocular fields and wide lateral fields, reflecting their specialization for long-distance prey detection (Tucker, 2000; O'Rourke et al., 2010). Figure 1 provides a generalized schematic overview of the main components of avian vision.

In comparison to human eyes, which have only a single shallow central fovea, avian vision (e.g., raptors, swallows, and terns) possesses, in addition to a shallow temporal fovea, a deep central fovea. This deep fovea provides image magnification and motion tracking, enabling detection and tracking of distant targets. Whereas human eyes are limited to the visible spectrum, avian eyes possess four cone types sensitive to ultraviolet (UV) and visible light. This UV sensitivity allows birds to distinguish targets from complex backgrounds due to strong UV scattering from object surfaces (Cuthill et al., 2000). Moreover, birds, especially those from the raptor family, have a wider field of view ($\sim$ 250°– 270°) than humans ($\sim$210°), but a smaller binocular area ($\sim$30°– 36°) than humans ($\sim$120°), which helps them better focus on a target while preserving a wide contextual field. Additionally, avian vision is at least four times sharper than human vision (Strasburger and Pöppel, 2002; Martin, 2007, 2009; O'Rourke et al., 2010; Strasburger et al., 2011; Potier et al., 2018; Miñano et al., 2023). Hence, these benefits can improve human vision abilities for specific applications. For instance, Park et al. (2024) introduced an avian-inspired vision system that magnifies remote objects and improves target-background discrimination in dynamic conditions by performing foveated imaging for remote target detection.

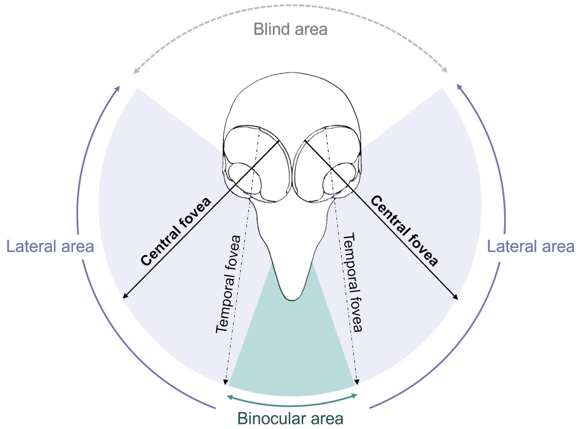

Figure 1. Avian vision schematic overview.

2.2 Cutaway representation

The roots of 3D cutaway representation trace back to the work of Feiner and Seligmann (1992), who introduced the obscuring-object cutaway — a technique that renders by cutting away parts of blocking objects to fully reveal the object behind. Over time, the technique was developed, extended with visual variables, and applied across diverse fields, such as medicine, biology, geology, architecture, and computer graphics (Bruckner et al., 2005; Li et al., 2007; McInerney and Crawford, 2010; Lidal et al., 2012; Muzic et al., 2016; Li et al., 2025). As a vivid example of this development, Viola et al. (2004) presented a cutaway through importance-driven volume rendering of interior structures using transparency and color saturation to reveal the area of cut. Wang et al. (2005) introduced the magic volume lens as an interactive "focus+context" method for volume rendering, representing a cutaway along with magnified cut features using circular, square, and arbitrary-shaped lenses. Burns and Finkelstein (2008) created object-defined cutaways, where the cutaway shape is determined solely by the objects of interest and changes with viewpoint.

Elmqvist and Tsigas (2008) formalized the design space of 50 occlusion management techniques, including 3D cutting planes, object removal, perspective cutouts, view-dependent transparency, occlusion-free route animation, and others, by developing a taxonomy and deriving five orthogonal design patterns: volumetric probes, projection distorters, virtual X-ray, tour planners, and multiple views. Volumetric probes apply object-space deformations based on spatial probes manipulated by the user. Projection distorters combine multiple projection views to maximize target visibility. Virtual X-ray reveals targets by making occluders transparent or invisible. Tour planners employ a fixed or auto-generated camera route that moves between targets. Multiple views provide effective occlusion reduction in 3D environments. These techniques laid the foundation for cutaway visualization and remain widely used in modern UDT applications. For instance, Konev et al. (2018) introduced dynamic cutaways revealing underground sewer networks and occluded water as users zoom from city overview to close-up. Rauer-Zechmeister et al. (2024) proposed removing neighboring occluding buildings with cutting planes to expose a focus building during flood simulation, while preserving structural lines for context. Mota et al. (2026) described an occlusion-free lens integrating temporal displays on building footprints, removing self-occluding geometry for an unobstructed view and coloring cut edges with layered ribbons encoding distinct time instances. Grounded in these insights and inspired by the avian eye, this paper introduces dynamic object-adapted cutaway with additional visual variables for focus object observation.

3. Methodology

3.1 Bio-inspired cutaway design

Based on the avian vision benefits outlined in Section 2.1, we draw an analogy between a raptor's visual focus on its prey and a user's observation of a target object within a 3D urban scene. Therefore, it is proposed to divide the field of view of the scene into components analogous to avian vision: the target area that includes an object and its vicinity represents the narrow central fovea region, the area around it is set as binocular, and the rest of the field is lateral (peripheral). Each of these components is characterized by specific visual acuity, which can be interpreted by the Level-of-Details (LODs) in the voxel scene. That is why the view is represented within three LODs, while the other field characteristics are interpreted through visual variables.

In our design, the target object and its immediate surroundings are considered the primary focus and, therefore, must remain visible from any viewpoint. Consequently, the cutaway is applied to all occluding geometry to ensure their unobstructed observation. This focal area corresponds to the central fovea region and is therefore represented by the highest LOD2. Additionally, the magnification ability of this field is realized as a lens effect.

To preserve scene context during observation, the area around the cut, which corresponds to the binocular field, is represented with LOD1 and reinforced by a dark tint that increases with distance from the target, interpreting the depth perception of binocular vision. The remainder of the scene, the lateral field, which has the lowest acuity, is presented with LOD0.

Figure 2 shows a schematic cross-section of the view frustum with the three observation regions: central fovea, binocular, and lateral (peripheral). The focus object is shown as a red rectangle, while the cut area containing occluders is shown in blue.

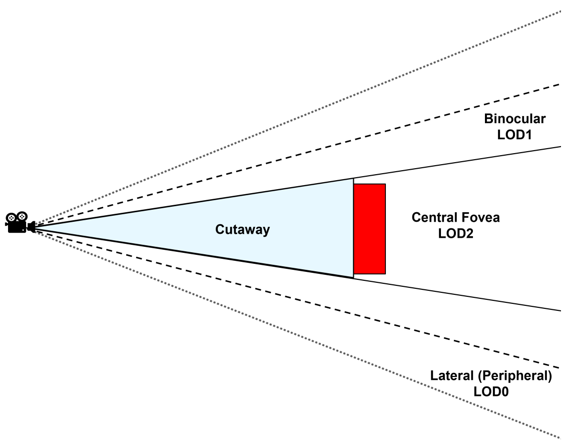

Figure 2. Cross-section of the view frustum for the bio-inspired cutaway visualization.

The avian ability to distinguish targets from complex backgrounds, enabled by UV sensitivity, is interpreted through the interplay of color contrast and value adjustment: the focus object and its immediate surroundings (the central fovea region) receive increased color intensity, the binocular area receives decreased intensity, and the lateral area is rendered in grayscale to reduce visual attention, analogous to the peripheral vision of birds.

3.2 Dataset

To derive the 3D voxel-based representation, the high-accuracy dense point cloud acquired with the Riegl VMX-250 Mobile Mapping System (MMS) was used. The dataset covers an area of approximately 340 by 240 meters in Hannover, Germany, and comprises almost 70 million points.

In the next step, the point cloud is classified using the Kernel-Point Convolution (KPConv) approach (Thomas et al., 2019), yielding 12 semantic classes: Building, Road, Fence, Person, Pole, Traffic Sign, Tree Top, Tree Trunk, Bush, Terrain, Bicycle, and Car. Subsequently, the point cloud is integrated into a regular 3D grid at 10 cm resolution to generate LOD2 for the cutaway visualization. Corresponding LOD1 (40 cm voxel size) and LOD0 (80 cm voxel size) are derived from LOD2, following the analogy of the avian vision regions described in subsection 3.1. For the cutaway application, a person captured during the point cloud acquisition is selected as the focus object.

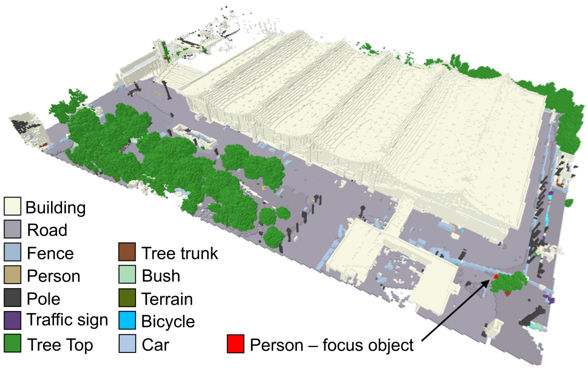

Figure 3. Voxel-based representation (LOD0).

Figure 3 demonstrates the derived 80 cm voxel representation of the dataset, colorized according to the classification results, with the focus object highlighted in red.

3.3 Cutaway implementation

For the implementation of the bio-inspired cutaway visualization, the cross-browser JavaScript library Three.js is employed. This platform provides a comprehensive set of rendering capabilities for real-time 3D visualization on the web, including custom shader programming, instanced rendering, and LOD management, all of which are essential for the development of the cutaway technique for a voxel-based environment.

The 3D voxel scene is generated from the voxelized point cloud for each LOD using instanced meshing, which optimizes rendering of large numbers of voxels. The cutaway is then calculated for each frame to ensure an unobstructed view on the focal area during dynamic camera movement. The implementation, composed of three areas (central fovea, binocular, and lateral), is described in detail in the following subsections.

3.3.1 Central fovea: According to the design described in Section 3.1, the fovea region defines a cutaway of the occluding geometry (in our case, voxels) and incorporates an LOD2 representation for detailed observation of the focal area (the focus object and its surroundings). Additionally, it includes magnification of this area, emphasized using enhanced color intensity. Considering the avian vision fovea field described in Section 2.1, the fovea zone is defined as a cone frustum with a corresponding half-cone angle of 1°, denoted as θ_{fovea}. However, to capture not only the object but also its vicinity at close distances, θ_{fovea} is calculated as:

$$\theta_{\text{fovea}} = \max\left(1^\circ,\ \arctan\left(\frac{n \cdot D}{h}\right)\right), \tag{1}$$

where n = surrounding gain coefficient
D = diagonal of the object's bounding box
h = distance to the focus object

Drawing from the avian eye characteristic, the general parameter θ_{fovea} (initially 1°) could be increased to enlarge the focal area if necessary.

Parameter n regulates how much of the focus object's surroundings are included in the focal area. It is suggested that $n > 0.5$, ensuring that the object is at least seen entirely with minimum surrounding. If more surrounding than the diagonal D measure can provide is required, then $n > 1$ should be used.

Based on θ_{fovea} the cone frustum is constructed, extending through the focus object and continuing beyond it to encompass its surroundings. The cone radius at any point along the cone axis is defined as:

$$r_{\text{fovea}} = h \cdot \tan(\theta_{\text{fovea}}) \tag{2}$$

In the vertex shader, the frustum is further used for LOD assignment and magnification. To determine whether a voxel belongs to the fovea region, the perpendicular distance d from the voxel position to the cone axis is calculated as:

$$d = \|\mathbf{P} - \mathbf{O}\|, \tag{3}$$

where O = the closest point on the cone axis
P = voxel position

If the condition $d \leq r_{\text{fovea}}$ is true, the voxel is represented with the smallest voxel size of 10 cm (LOD2). Furthermore, a magnification effect is applied to voxels in the fovea region (LOD2) to enhance the visibility of the focal area when observed from a far distance. Figure 4 illustrates the cone frustum defining the fovea region.

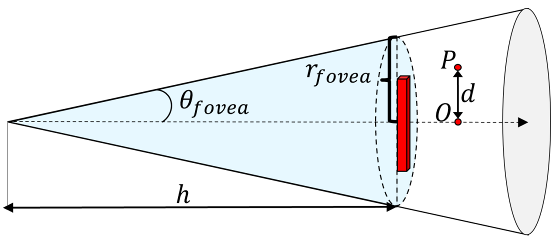

Figure 4. Cone frustum of the fovea region.

The magnification strength is determined by two factors: h and d. The distance factor t, which represents the normalized distance from the camera, is computed as:

$$t = \min\left(\frac{h}{h_c}, 1\right), \tag{4}$$

where h_c = magnification distance constant

h_c is a tunable distance threshold that constrains the maximum strength of object magnification at that distance. Its choice depends on the desired visual effect on the object. In our scene, it was set to 50. The lens strength is then calculated using an exponential growth function:

$$S_{\text{dist}} = 1 - \exp\left(-k \cdot t^2\right), \tag{5}$$

where k = adjustable growth rate of magnification

This results in a gradual increase in magnification applied to the vertices of voxels as the viewing distance increases. The choice of parameter k depends on the desired magnification strength, which is determined by the visual effect on the object and can differ across focus object shapes, types, and other properties. In our experiment, it is set to 9. Additionally, for a smooth transition at the boundaries of the fovea cone, a radial falloff R is applied as:

$$R = 1 - 3\left(\frac{d}{r_{\text{fovea}}}\right)^2 + 2\left(\frac{d}{r_{\text{fovea}}}\right)^3, \tag{6}$$

with $R = 1$ at $d = 0$ and $R = 0$ at $d = r_{\text{fovea}}$. Therefore, the focus object receives the maximum magnification effect, while the magnification of its surroundings smoothly decreases toward the boundaries of the fovea cone. The final lens magnification therefore defined as:

$$S_{\text{lens}} = S_{\text{dist}} \cdot R \tag{7}$$

Similarly, the frustum is used in the fragment shader. Voxels within the fovea region between the camera and the focus object are discarded, effectively performing the cutaway. The cutaway volume of the cone is highlighted in blue in Figure 4. Therefore, magnified voxels that meet the condition $d \leq r_{\text{fovea}}$ belong to the surroundings of the focus object (located inside the white volume of the cone in Figure 4), and the object itself (the red rectangular prism in Figure 4) remain visible and receive a 20% brightness boost, enhancing contrast and drawing attention to the focal area.

3.3.2 Binocular: For the binocular area another cone frustum is built similar to the central fovea. In this case, the half cone angle $\theta_{\text{binocular}}$ is set to 15°, following the binocular field angular size of around 30°(see Section 2.1). Hence, the cone radius $r_{\text{binocular}}$, is derived analogously to equation 2 as:

$$r_{\text{binocular}} = h \cdot \tan(\theta_{\text{binocular}}) \tag{8}$$

Consequently, voxels that satisfy $r_{\text{fovea}} < d \leq r_{\text{binocular}}$ are assigned LOD1 in the vertex shader and rendered with 40 cm size. In the fragment shader, the color intensity of these voxels is reduced by blending the original color with black at 30% strength to express the contrast between the focal area and the binocular region. Furthermore, for voxels within the binocular region that lie in front of the target, a radial halo transparency effect is applied. This effect creates a ring around the cut of transparent voxels, whose opacity increases in the direction away from the cut. This visual variable aims to improve cutaway perception while revealing the surrounding context through semi-transparent voxels around the cutaway. The halo width is dynamically scaled based on the distance h as follows:

$$h_w = \max\left(h_{\min}, \min(h, h_{\max})\right), \tag{9}$$

where $h_{\min}$ = min distance for halo scaling
$h_{\max}$ = max distance for halo scaling

h_{min} and h_{max} tuning constraints that help control transparency presentation and growth, set to 0.5 and 15 with regard to visual performance for the scene. Further, the clamped distance h_{w} is linearly mapped to a percentage p, which defines the fraction of the binocular ring width occupied by the halo. The halo width is then calculated as:

$$w = p \cdot (r_{\text{binocular}} - r_{\text{fovea}}), \tag{10}$$

The radial transparency value α of the voxel is linearly interpolated between α_{min} and 1.0 and modulated as:

$$\alpha = (1 - b) \cdot \alpha_{\text{min}} + b \cdot 1.0, \tag{11}$$

where b = interpolation factor
α_{min} = minimum opacity level

While the interpolator factor b is defined as:

$$b = \begin{cases} 0 & u \le 0 \\ 3u^2 - 2u^3 & 0 < u < 1 \\ 1 & u \ge 1 \end{cases}, \quad \text{with} \quad u = \frac{d - r_{\text{fovea}}}{w} \tag{12}$$

Additionally, a halo region is used to apply a dark tint. As proposed in Section 3.1, the depth perception of the binocular field in avian vision is interpreted as a dark tint for distant observations. Therefore, a tint strength is defined as:

$$s = f \cdot (1 - b), \quad \text{with} \quad f = \frac{h_{\text{w}} - h_{\text{min}}}{h_{\text{max}} - h_{\text{min}}} \tag{13}$$

3.3.3 Lateral (peripheral): The rest of the 3D scene, consisting of voxels with $d > r_{\text{binocular}}$, is considered the lateral (peripheral) region. It is rendered as 80 cm voxels (LOD2) in the vertex shader and colored in grayscale in the fragment shader.

4. Results

4.1 Bio-inspired cutaway visualization

This section presents the bio-inspired cutaway applied to observe a focus object - the voxel-represented person (Section 3.2) from various viewpoints. Figure 5 (a) shows a 10 m view: a circular cut through the blue fence reveals the red object at 10 cm voxels (via LOD), enabling perception of a walking person, while surroundings remain coarser (40 and 80 cm). A color gradient maps three perceptual zones: fovea with increased brightness, binocular with decreased intensity, and lateral in grayscale. A transparent halo softens the cut boundary to reveal context. Figure 5 (b) demonstrates the cutaway from 30 m: the red object and surroundings retain detailed, intense representation despite the threefold distance increase, while the transparent halo widens as a multiple-layer occluder cutaway extending beyond the yellow building wall. Figure 5 (c) presents the cutaway from 180 m without and with zoom (red frame). Without zoom, the red object remains recognizable as a silhouette, and a dark tint added to the halo simulates a spotting scope effect to enhance depth perception in the binocular zone (Section 3.3.2). Applying zoom exposes the fovea magnification effect (Section 3.3.1), enlarging the red person most with diminishing enlargement toward the cutaway borders. While the silhouette remains perceivable without zoom, the zoomed view enables perception of details of both the person and surroundings (e.g., blue fence, violet traffic sign) even at 180 m.

4.2 User evaluation survey

4.2.1 Survey design and procedure: To evaluate the bio-inspired cutaway, we conducted a 19-item user survey: 5 general questions and 14 visualization-specific tasks. Figure 6 illustrates the question sequence and image allocation — each item is labeled "Q", general questions appear in plain frames, and visualization items include representative imagery.

The survey consisted of the following items:

General questions (Q1–Q4, Q19) captured demographic and background information: age group, emergency services experience, 3D modeling/visualization experience, gaming frequency, and self-reported visual impairment.

Visualization tasks (Q5–Q18) evaluated perception and understanding of the bio-inspired cutaway and 3D voxel scene in general, as well as the functionality and additive value of each visual feature, including varying LOD, color contrast, transparency halo, magnification, and dark tint, with regard to focus object observation. The bio-inspired cutaway was compared against a standard cutaway of the same size without the visual variable extensions and with only 80 cm LOD. The visual features were added one by one sequentially with each next question (images with additive features are marked with * in Figure 6). For every comparison, participants chose which image performed better and rated both images on a 1–5 scale. The tasks comprised scene objects identification (Q5), recognition of the revealed object as a person with and without LOD (Q6–Q7), successive enhancements (LOD, color contrast, transparency halo at 10 m and 30 m, magnification, and dark tint) evaluating ease of understanding, focusing, and perception (Q8-Q14), interactive video comparisons of standard versus bio-inspired cutaways assessing focus, detail perception, obstacle awareness, and person recognition (Q15–Q17), and a final far-distance zoomed comparison evaluating informativeness (Q18).

4.2.2 Survey results: The user survey was conducted with 23 participants, with a mean age of 32 years (SD = 8.4 years), indicating a diverse adult sample. Answers for Q5 revealed that, on average, participants correctly identified 5.35 out of 6 objects on the 80 cm voxel scene, achieving 89.2% accuracy in a voxel scene understanding. In Q6, only 4.3% of users could recognize a red object as a person with the standard cutaway, while in Q7, 100% of participants recognized a person when the LOD feature was added to the cutaway. Figure 7 presents the results of the side-by-side image and video comparison tasks of Q8–Q14 and Q16–Q18. Preference for extended visualizations with LOD, color contrast, transparency halo, and dark tint (marked with * in Figure 6) is shown in green, while standard cutaway and versions with fewer variables are highlighted in red. More than half of participants acknowledged that all bio-inspired features have additive value and preferred the bio-inspired visualization. LOD outperformed the standard cutaway in terms object understanding (Q8). Magnification for far-distance observation achieved 100% effectiveness for focal area observation (Q13). Transparency halo preference increased from 56.5% at 10 m (Q11) to 69.6% at 30 m (Q12).

Table 1 provides descriptive statistics for all rating questions, with the most notable values highlighted in bold. The results

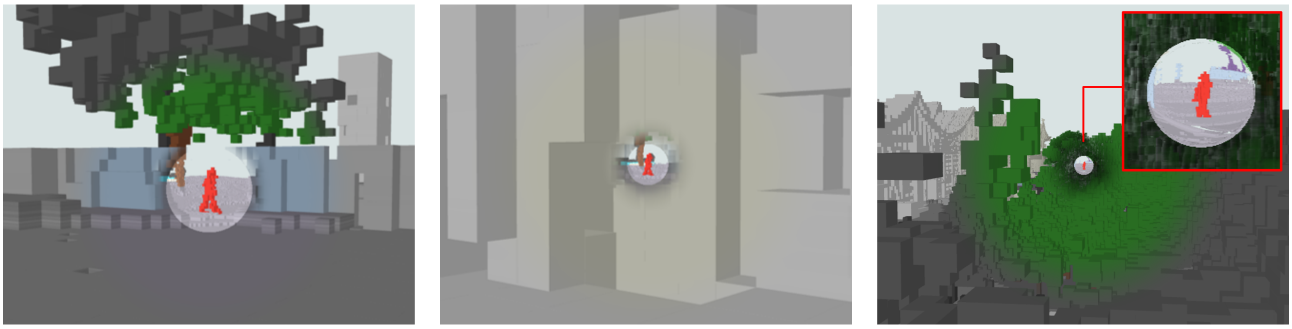

(a) 10 m observation distance (b) 30 m observation distance (c) 180 m observation distance

Figure 5. Bio-inspired cutaway visualization.

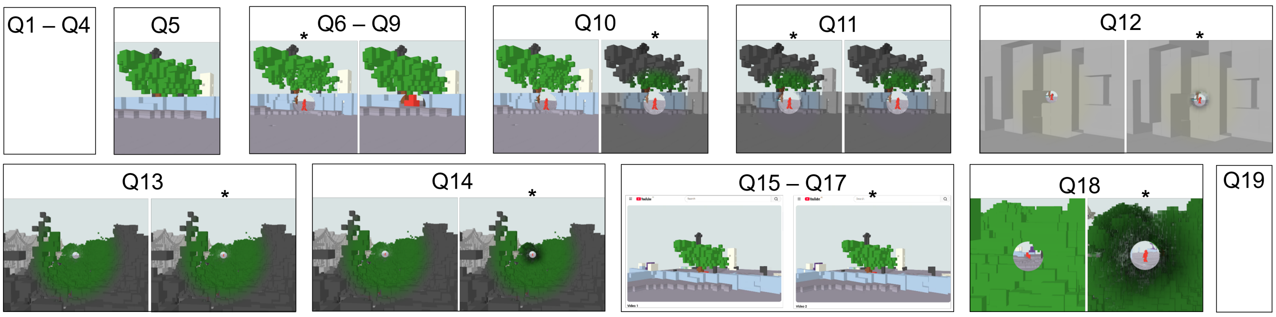

Figure 6. Overview of the user survey layout, including question sequence and image allocation for visualization tasks.

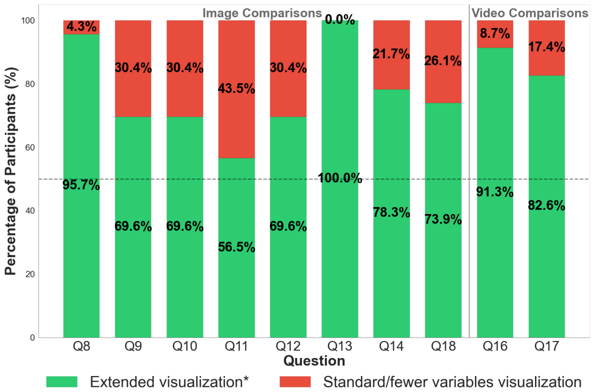

Figure 7. User preference results for image and video comparison tasks (Q8–Q14 and Q16–Q18).

Question	Mean	SD	Min. rate	Max. rate
Q8*	**3.87**	**1.06**	**1**	**5**
Q8	**1.65**	**1.11**	**1**	**5**
Q9*	**3.74**	**1.14**	**2**	**5**
Q9	**3.52**	**1.53**	**1**	**5**
Q10	3.70	1.02	1	5
Q10*	3.74	1.25	1	5
Q11*	**3.74**	**0.96**	**1**	**5**
Q11	**4.00**	**0.85**	**1**	**5**
Q12	3.13	1.10	1	5
Q12*	3.26	1.18	1	5
Q13	**1.52**	**0.73**	**1**	**3**
Q13*	**3.39**	**1.12**	**1**	**5**
Q14	**4.04**	**0.88**	**2**	**5**
Q14*	**4.09**	**0.67**	**3**	**5**
Q16	2.83	1.15	1	5
Q16*	3.91	1.16	1	5
Q17.1	2.57	1.38	1	5
Q17.1*	3.35	1.50	1	5
Q17.2	2.17	1.19	1	4
Q17.2*	3.83	1.03	1	5
Q18	2.13	1.32	1	5
Q18*	3.39	1.34	1	5

Table 1. Descriptive statistics for all rating questions.

corresponding to the extended visualizations with extra features and the bio-inspired cutaway are marked with *, similar to the markings in Figure 6 and Figure 7. In general, the ratings show the same tendency of extended features and bio-inspired cutaway visualization outperforming the representations with fewer features and the standard representation. However, it can be noticed that despite 69.6% preference for the LOD-featured cutaway in terms of better object focusing (Q9 in Figure 7), the ratings show a very small mean difference of 0.22 and high standard deviation (SD) values. This signals a small additive value of the LOD feature in terms of helping to focus on the object, as well as a high level of disagreement among participants' answers.

Another interesting finding is that despite 56.5% preference for the cutaway with transparency halo over 43.5% without it (Q11 in Figure 7), the mean rating without the halo was 0.26 higher than with it (Q11, Q11* in Table 1), suggesting that the halo at close distance does not sufficiently support cutaway perception. LOD again performed best for scene understanding (Q8* vs Q8), while magnification excelled for far-distance object observation (Q13 vs Q13*). However, despite magnification being the most preferred feature (Q13 in Figure 7), LOD achieved the highest additive value in rating tasks (2.22). One additional point to note concerns the rating results of Q14 and Q14*, despite 78.3% preference for dark tint for better observation (Q14 in Figure 7), it had almost no additive value for depth perception. No significant differences were found based on prior 3D visualization experience or edge group affiliation. The number of participants from emergency-related fields (2) and those with vision issues (1) was insufficient for statistical analysis.

However, participants who play video games at least sometimes (52%) showed a stronger tendency to recognize the additive value of the visual features.

5. Conclusion and Outlook

This work presented a bio-inspired cutaway visualization approach for voxel-based urban digital twins, drawing an analogy between a raptor's visual focus on prey and a user's observation of a target object in a 3D urban scene. The design integrates the cutaway enhanced by multiple visual features designed to improve ease of object observation: LOD for object identification and focal area detail, color contrast for focal area concentration, a transparency halo for cutaway context, dark tint for depth perception and focus, and magnification for distant observation. These features were evaluated through a 19-item user survey with 23 participants.

The evaluation confirmed that the bio-inspired cutaway consistently outperformed the standard cutaway. The LOD feature demonstrated the highest additive value, achieving the largest rating improvement of 2.22 for scene understanding and enabling 100% of participants to recognize a person as a focus object versus only 4.3% recognition with the standard cutaway. Magnification proved equally effective for far-distance observation. Color contrast provided moderate benefits, while the transparency halo showed mixed results with low rating at close distance observation. Dark tint, despite 78.3% preference, offered almost no additional benefit for depth perception.

Although the bio-inspired cutaway performed better than the standard one and its visual features demonstrated additive value for scene observation, the moderate average rating of 3.66 out of 5 suggests that there is still room for further improvement. It is worth noting that the colors and shapes of the surrounding or occluding environment might influence the effectiveness of the proposed visualization variants, as well as the color choice of the focus object. These factors could have also affected user responses in the survey. Importantly, the parameters n, h_c, k, h_{min}, h_{max} introduced in Section 3.3 allow the visualization to be adjusted to achieve the desired effect across diverse 3D scenes. Therefore, future work will prioritize optimizing the transparency halo and dark tint features, conducting more experiments on possible visualizations, and exploring additional visual variables. Furthermore, it will include experiments with non-circular cut shapes, testing the cutaway in diverse scenes, and revising the visualization design using insights from video game techniques. Alternative interactive scenarios (moving objects, static/dynamic cameras) and multi-object observation benefits of avian vision will also be investigated, alongside larger-scale user studies to benchmark performance against existing approaches.

References

Azadi, S., Kasraian, D., Nourian, P., van Wesemael, P., 2025. What have urban digital twins contributed to urban planning and decision making? from a systematic literature review toward a socio-technical research and development agenda. *Int. Arch. Photogramm. Remote Sens. Spatial Inf. Sci.*, 8number 1, 32.

Bruckner, S., Grimm, S., Kanitsar, A., Gröller, E., 2005. Illustrative Context-Preserving Volume Rendering. *VisSym / EuroVis05*, 69–76.

Burns, M., Finkelstein, A., 2008. Adaptive cutaways for comprehensible rendering of polygonal scenes. *ACM SIGGRAPH Asia 2008 Papers*, Association for Computing Machinery, New York, NY, USA.

Cárdenas-León, I., Koeva, M., Nourian, P., Davey, C., 2024. Urban digital twin-based solution using geospatial information for solid waste management. *Sustainable Cities and Society*, 115, 105798.

Cornel, D., Buttinger-Kreuzhuber, A., Konev, A., Horváth, Z., Wimmer, M., Heidrich, R., Waser, J., 2019. Interactive Visualization of Flood and Heavy Rain Simulations. *Computer Graphics Forum*, 38(3), 25–39.

Cuthill, I. C., Partridge, J. C., Bennett, A. T. D., Church, S. C., Hart, N. S., Hunt, S., 2000. Ultraviolet Vision in Birds. *Advances in the Study of Behavior*, 29, 159–214.

Elmqvist, N., Tsigas, P., 2008. A Taxonomy of 3D Occlusion Management for Visualization. *IEEE Transactions on Visualization and Computer Graphics*, 14(5), 1095–1109.

Feiner, S. K., Seligmann, D. D., 1992. Cutaways and ghosting: satisfying visibility constraints in dynamic 3D illustrations. *The Visual Computer*, 8, 292–302.

Ferré-Bigorra, J., Casals, M., Gangolells, M., 2022. The adoption of urban digital twins. *Int. Arch. Photogramm. Remote Sens. Spatial Inf. Sci.*, 131, 103905.

Gorte, B., 2023. Analysis of very large voxel datasets. *International Journal of Applied Earth Observation and Geoinformation*, 119, 103316.

Grieves, M., Vickers, J., 2017. Digital Twin: Mitigating Unpredictable, Undesirable Emergent Behavior in Complex Systems. *Transdisciplinary Perspectives on Complex Systems*, 85–113.

Heeramaglore, M., Kolbe, T. H., 2022. Semantically Enriched Voxels as a Common Representation for Comparison and Evaluation of 3D Building Models. *ISPRS Annals of the Photogrammetry, Remote Sensing and Spatial Information Sciences*, X-4/W2-2022, 89–96.

Knödel, S., Guitton, P., 2009. Interactive Generation and Modification of Cutaway Illustrations for Polygonal Models. *Lecture Notes in Computer Science*, 5531, 140–151.

Koncicki, A., Pietruszyńska, M., Mieszczak, M., Stępniewska, J., Tykałowski, B., Stenzel, T., 2025. Selected issues in the anatomy and physiology of the avian organ of vision and eye disorders in farmed poultry. *Journal of Veterinary Research*, 69(2), 241–247.

Konev, A., Matusich, M., Viola, I., Schulze, H., Cornel, D., Waser, J., 2018. Fast cutaway visualization of sub-terrain tubular networks. *Computers & Graphics*, 75, 25–35. https://doi.org/10.1016/j.cag.2018.07.004.

Lehner, H., Dorffner, L., 2020. Digital geoTwin Vienna: Towards a Digital Twin City as Geodata Hub. *PFG — Journal of Photogrammetry, Remote Sensing and Geoinformation Science*, 88, 63–75.

Li, W., Ritter, L., Agrawala, M., Curless, B., Salesin, D., 2007. Interactive cutaway illustrations of complex 3D models. *ACM Transactions on Graphics*, 26(3), 31.

Li, X., Jalan, P., Dingliana, J., 2025. The design and evaluation of a tangible interface for cutaway visualization in Mixed Reality. *Computers & Graphics*, 133, 104454.

Lidal, E. M., Hauser, H., Viola, I., 2012. Design principles for cutaway visualization of geological models. *Proceedings of the 28th Spring Conference on Computer Graphics*, Association for Computing Machinery, New York, NY, USA, 47–54.

Martella, A., Ramadan, A., Martella, C., Patano, M., Longo, A., 2023. State of the art of urban digital twin platforms. *Extended Reality. XR Salento 2023. Lecture Notes in Computer Science*, 14218, Springer, Cham, 299–317.

Martin, G. R., 2007. Visual fields and their functions in birds. *Journal of Ornithology*, 148(Suppl 2), 547–562.

Martin, G. R., 2009. What is binocular vision for? A birds' eye view. *Journal of Vision*, 9(11), 14.1–19.

McInerney, T., Crawford, P., 2010. Ribbonview: Interactive context-preserving cutaways of anatomical surface meshes. *Advances in Visual Computing (ISVC 2010)*, Lecture Notes in Computer Science, 6454, Springer, Berlin, Heidelberg, 533–544.

Miñano, S., Golodetz, S., Cavallari, T. et al., 2023. Through Hawks' Eyes: Synthetically Reconstructing the Visual Field of a Bird in Flight. *International Journal of Computer Vision*, 131, 1497–1531. https://doi.org/10.1007/s11263-022-01733-2.

Mortazavi, F. S., Shkedova, O., Feuerhake, U., Brenner, C., Sester, M., 2023. Voxel-based Point Cloud Localization for Smart Spaces Management. *The International Archives of the Photogrammetry, Remote Sensing and Spatial Information Sciences*, XLVIII-1/W1-2023, 325–332. http://dx.doi.org/10.5194/isprs-archives-XLVIII-1-W1-2023-325-2023.

Mota, R., Silva, J. D., Miranda, F., Alim, U., Sharlin, E., Ferreira, N., 2026. Occlusion-Free Conformal Lensing for Spatiotemporal Visualization in 3D Urban Analytics. *arXiv preprint arXiv:2602.03743*.

Muzic, M. L., Mindek, P., Sorger, J., Autin, L., Goodsell, D., Viola, I., 2016. Visibility Equalizer Cutaway Visualization of Mesoscopic Biological Models. *Computer Graphics Forum*, 35(3), 161–170.

O'Rourke, C. T., Hall, M. I., Pitlik, T., Fernández-Juricic, E., 2010. Hawk Eyes I: Diurnal Raptors Differ in Visual Fields and Degree of Eye Movement. *PLOS ONE*, 5(9), e12802. https://doi.org/10.1371/journal.pone.0012802.

Park, J., Kim, M. S., Kim, J., Chang, S., Lee, M., Lee, G. J., Song, Y. M., Kim, D.-H., 2024. Avian eye–inspired perovskite artificial vision system for foveated and multispectral imaging. *Science Robotics*, 9(90), eadk6903. https://www.science.org/doi/abs/10.1126/scirobotics.adk6903.

Potier, S., Bonadonna, F., Martin, G. R., Isard, P.-F., Dulaurent, T., Mentek, M., Duriez, O., 2018. Visual configuration of two species of Falconidae with different foraging ecologies. *Ibis*, 160(1), 54–61.

Raes, L., Michiels, P., Volckaert, B., Turck, F. D., 2022. DUET: A Framework for Building Interoperable and Trusted Digital Twins of Smart Cities. *IEEE Internet Computing*, 26(3), 43–50.

Rauer-Zechmeister, S., Cornel, D., Sadransky, B., Horváth, Z., Konev, A., Buttinger-Kreuzhuber, A., Heidrich, R., Blöschl, G., Gröller, E., Waser, J., 2024. HORA 3D: Personalized Flood Risk Visualization as an Interactive Web Service. *Computer Graphics Forum*, 43(3), e15110.

Ruohomäki, T., Kesäniemi, O., Airaksinen, E., Martikka, M., Huuska, P., Suomisto, J., 2018. Smart City Platform Enabling Digital Twin. *IEEE*.

Schrotter, G., Hürzeler, C., 2020. The Digital Twin of the City of Zurich for Urban Planning. *PFG – Journal of Photogrammetry, Remote Sensing and Geoinformation Science*, 88(1), 99–112.

Shen, Y., Zhou, J., Wang, S., Chen, Y., Liu, J., 2025. Research on 3D visual condition monitoring of marine bracket based on digital twin. *Journal of Physics: Conference Series*, 2951(1), 012081.

Strasburger, H., Pöppel, E., 2002. Visual field. G. Adelman, B. H. Smith (eds), *Encyclopedia of Neuroscience*, 3rd edn, Elsevier Science B.V., Amsterdam, New York. on CD-ROM.

Strasburger, H., Rentschler, I., Jüttner, M., 2011. Peripheral vision and pattern recognition: A review. *Journal of Vision*, 11(5), 13.

Sukma, A. I., Koeva, M. N., Reckien, D., Bočkarjova, M., Mano, A. D. S., Canilli, G., Vicentini, G., Kerle, N., 2024. 3d city digital twin simulation to mitigate heat risk of urban heat islands. *Proceedings of the 19th 3D GeoInfo Conference 2024*, 4/W11-2024, Copernicus, Vigo, 129–136. Conference: 19th 3D GeoInfo Conference 2024, Vigo, Spain, 1–3 July 2024.

Thomas, H., Qi, C. R., Deschaud, J.-E., Marcotegui, B., Goulette, F., Guibas, L. J., 2019. Kpconv: Flexible and deformable convolution for point clouds. *Proceedings of the IEEE/CVF International Conference on Computer Vision (ICCV)*, 6511–6520.

Tucker, V. A., 2000. The deep fovea, sideways vision and spiral flight paths in raptors. *Journal of Experimental Biology*, 203(Pt 24), 3745–3754.

Viola, I., Kanitsar, A., Groller, M. E., 2004. Importance-driven volume rendering. *IEEE Visualization 2004*, 139–145.

Vujasinović, S., Becker, S., Breuer, T., Bullinger, S., Scherer-Negenborn, N., Arens, M., 2020. Integration of the 3D Environment for UAV Onboard Visual Object Tracking. *Applied Sciences*, 10(21), 7622.

Wang, L., Zhao, Y., Mueller, K., Kaufman, A., 2005. The magic volume lens: an interactive focus+context technique for volume rendering. *VIS 05. IEEE Visualization, 2005*, 367–374.

Wang, X., Ma, L., Xiong, J., 2026. Research on a Smart Fire Monitoring System for University Dormitories Based on Edge-Cloud Collaboration and Digital Twin Technology. *Frontiers in Computing and Intelligent Systems*, 15(3), 147–160.

Xu, H., Zlatanova, S., Liang, R., Canbulat, I., 2026. A Modular Light-weight Voxel-Based 3D Wildfire Propagation Simulator in Python Using LiDAR Data, High-Performance Computing (HPC), and Immersive Scientific Visualization. *ISPRS Annals of the Photogrammetry, Remote Sensing and Spatial Information Sciences*, X-3/W3-2025, 127–134.